RESEARCH ARTICLE

(Online First)Applying high-resolution visible imagery to satellite melt pond fraction retrieval: A neural network approach

Qi Liu[1], Yawen Zhang[1]
[1] University of Colorado, Boulder, CO, 80309

Abstract: During summer, melt ponds have a significant influence on Arctic sea-ice albedo. The melt pond fraction (MPF) also has the ability to forecast the Arctic sea-ice in a certain period. It is important to retrieve accurate melt pond fraction (MPF) from satellite data for Arctic research. This paper proposes a satellite MPF retrieval model based on the multi-layer neural network, named MPF-NN. Our model uses multi-spectral satellite data as model input and MPF information from multi-site and multi-period visible imagery as prior knowledge for modeling. It can effectively model melt ponds evolution of different regions and periods over the Arctic. Evaluation results show that the MPF retrieved from MODIS data using the proposed model has an RMSE of 3.91% and a correlation coefficient of 0.73. The seasonal distribution of MPF is also consistent with previous results.

Keywords: Multi-layer neural network; high-resolution imagery; melt pond fraction

1. Introduction

Melt ponds occur during the mealtime period of Arctic[1,2], influencing the sea ice albedo and solar energy partitioning on Arctic surface[3,4]. The availability of an accurate Arctic melt pond fraction (MPF) dataset is crucial to explore the melt pond evolution[5]. More importantly, it serves as an important parameter for Arctic climate study[6–8]. Because of better coverage both in observation areas and period[9], satellite remote sensing has become the main technique for Arctic MPF retrieval[10–14].

MPF retrieval algorithm plays an important role in producing a high-accuracy MPF dataset. Tschudi *et al*.[10] proposed a spectral unmixing procedure to retrieve MPF in Beaufort/Chukchi Sea region. This algorithm is based on a set of linear equations within four classes (melt pond, open water, snow, and bare ice). The reflectivity of different classes was measured near Barrow, Alaska in June, 2004 and fixed a priori in the equations. The mean difference between the satellite retrieved MPF and aerial observed MPF is 1.5%. Based on this algorithm, Rosel *et al*.[15] decreased it to three classes (melt pond, open water, and ice) while using similar equations to retrieve MPF. It should be noted that Rosel *et al*.[15] used the same fixed reflectivity as Tschudi *et al*.[10] and expanded the MPF retrieval results to the whole Arctic. Their results were validated with National Snow and Ice Data Center (NSIDC) melt pond data[16] at three sites, Beaufo for the Beaufort

Sea, Canadian for the Canadian Arctic and Cafram for the Fram Strait. The root-mean-square error (RMSE) was 10.7% and R-squared was 0.28. Tanaka *et al*.[9] also used some prior information from ship-based MPF to build a linear model between AMSR-E brightness temperature (TB) and MPF. As a result, their model can only be applicable to areas with high sea ice concentrations and RMSE is 8.9%.

Melt ponds are highly variable both in time and space[4,17], which may result in substantial errors in satellite MPF retrieval[18]. For MPF retrieval model, using fixed or inadequate prior knowledge for modeling could be problematic due

doi: 10.18063/som.v3i3.692

to the lack of generality for temporal and spatial variations[10]. A single site or period cannot represent the full range of melt pond variations, and using it as algorithm input could even impact the accuracy of retrieved MPF.

To improve the overall accuracy of satellite MPF retrieval model, we concentrate on two aspects in this paper: 1) the development of the MPF retrieval algorithm, 2) prior knowledge used in the model. For the algorithm part, we propose a multi-layer neural network based MPF retrieval model, which investigates the potential of using neural networks for spectral information extraction and building the relationship between satellite spectral information and MPF. For the prior knowledge part, we gather the high-resolution visible images from different regions and periods, then extract MPF information as prior knowledge for the proposed model. Previously, these high-resolution visible images were only used as validation or comparison source for satellite retrieved MPF[15,18,19]. Our main contributions are summarized as follows.

The development of the MPF-NN model, a novel satellite MPF retrieval model based on multi-layer neural network, with prior knowledge extracted from multi-site and multi-period high-resolution visible images.

Demonstration of the model's effectiveness in automatic feature extraction from multi-spectral satellite data and retrieving high-accuracy MPF over the Arctic sea ice.

Our paper is organized as follows. Section 2 presents the MPF-NN model and the data used in this work. Section 3 presents the results of model validation and retrieved MPF evolution over Arctic sea-ice. Section 4 discusses model observations and concludes this work.

2. MPE-NN: A neural network based satellite MPE retrieval model

Our MPF-NN model is developed with the goal of accurately retrieving MPF at various spatial and temporal scales. The accuracy of our model relies on: (1) the completeness of spatial and temporal coverage provided by high-resolution visible images, which serve as prior knowledge and training data for our model; (2) the quality of input data that are used to derive MPF, e.g., the reflectance of multiple bands from satellite data. The flowchart in **Figure 1** illustrates the development process of our MPF-NN model.

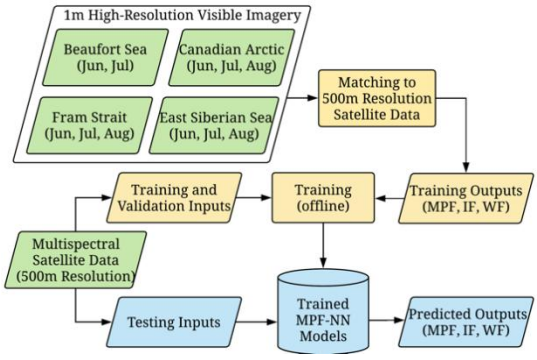

Figure 1. Design process of MPF-NN model.

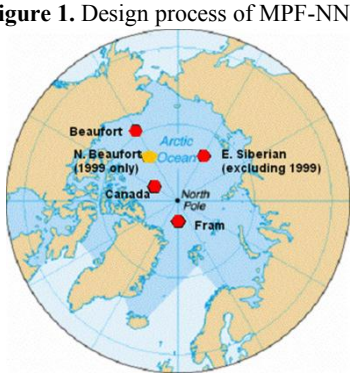

Figure 2. The Locations of four sites on Arctic sea (from NSIDC).

2.1 Data source for MPE-NN

Input Data: Our model utilizes multispectral satellite data as inputs. We select MODIS 500m daily surface reflectance products (MOD09GA) and use reflectance band 1 to 7 as model inputs. The wavelength of band 1-7 are

620-670nm, 841-876nm, 459-479nm, 545-565nm, 1230-1250nm, 1628-1652nm, and 2105-2155nm, respectively. All the cloud pixels in the daily product are removed.

Output Data: Our MPF-NN has three outputs: melt pond fraction (MPF), ice fraction (IF) and open water fraction (WF), which are derived from NSIDC melt pond imagery[16]. The NSIDC dataset came from a collection of high-resolution visible imagery, which was acquired over different Arctic sites during the summers of 1999, 2000, and 2001.

In this study, high-resolution images from four sites: Beau-fort Sea (73 N, 150 W), Canadian Arctic (85 N, 120 W), Fram Strait (85 N, 0 E) and East Siberian Sea (82 N, 150 E) in the summers of 2000 and 2001 are gathered as shown in **Figure 2.** In order to pair the input and output datasets, we re-project NSIDC imagery data to the Sinusoidal Projection (same as MOD09GA), down-sample the 1m resolution grids to 500m grids by averaging pixels values within a 500 500m grid and calculate the MPF, IF and WF in each grid corresponding to the grid of MOD09GA. In total, we train the model with 3,925 pairs of input and output data.

2.2 MPF-NN architecture

Our MPF-NN utilizes a multi-layer neural network architecture, which contains multiple hidden layers of units between the input and output layers[20], and is capable of extracting sophisticated features from input data and modeling non-linear input/output relationships[21,22]. As illustrated in **Figure 3**, the network has one input layer, M hidden layers, and one output layer. The input layer consists of N units, each hidden layer consists of S^M units and the output layer contains P units. A hyperbolic tangent (tanh) activation function is used after each hidden layer to capture the nonlinear relationship between the multi-spectral bands and the fractions of different surface classes. During model training and validating, back-ward propagation learning algorithm and adaptive moment estimation (ADAM) method are applied for optimizing the weights w and bias b before and after each hidden layer[23]. The nonlinear relationship between input x and y is represented in Eq.1, where f is an activation function after each hidden layer and output layer.

$$y = f^0(w^M \cdots f^2(w^2 f^1(w^1 x + b^1)) + b^2) + \cdots b^M)))) \quad (1)$$

Here, we briefly describe the design of our MPF-NN with an example of using MOD09GA data. We use a neural network with 3 hidden layers, each layer consisting of 7, 10, 10 units, respectively. The rationale behind this is: (1) we choose the number of units for each layer that is comparable with the number of input bands. For instance, all 7 bands of MOD09GA data are used as inputs, so we choose 7 or more units for each layer. (2) for the number of layers, we start from the simplest structure, i.e., 2 layers, then keep adding layers until the performance of the model stops improving. However, this empirical approach can lead to over-fitting with the incrementation of model depth, especially, when there are limited training data. In order to prevent over-fitting, each hidden layer is followed by a dropout layer. Dropout is a regularization technique to prevent over-fitting, which consists of randomly setting a fraction p of hidden layer units to 0 at each update during training[24]. The typical range of p is from 0.2 to 0.5. Empirically, we use 0.2 for the second and third hidden layers.

3. Results

We first validate the performance of our MPF-NN model on feature extraction and MPF retrieval accuracy. The results are compared with the MPF produced by the CICE hindcasts melt pond fraction model[8]. Finally, we analyze the retrieved MPF over the entire Arctic sea ice.

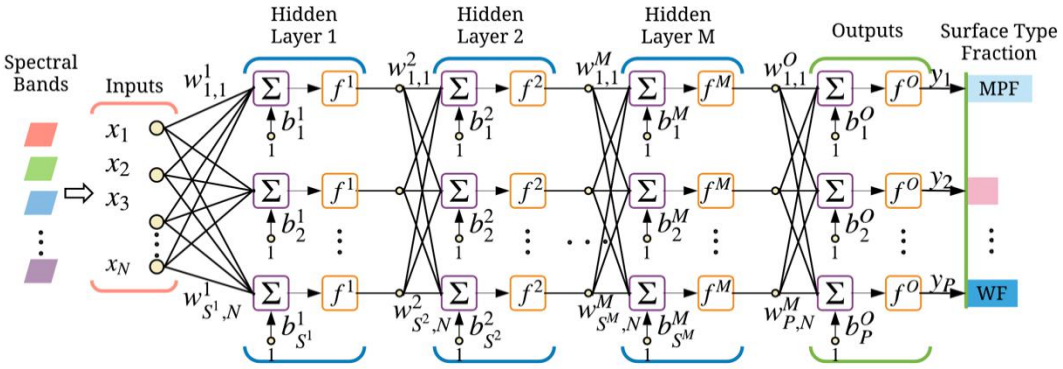

Figure 3. Illustration of a multi-layer neural network, which can be trained by a backward propagation learning algorithm through a series of layers. Inputs are reflectance from multi-spectral bands. Outputs are the fractions of multiple surface types, e.g., MPF, IF and WF.

3.1 Model validation

Feature Extraction: Typically, satellite imagery has multiple bands and hence it is essential to interpret how much each band contributes to the output, i.e., which bands are more important in differentiating melt ponds from ice and open water. Band 1, 2, 3 are utilized in the spectral unmixing algorithm[15,10]. In our MPF-NN model, all 7 bands from MOD09GA product are used to further improve the modeling accuracy. Here, we use MPF-NN to extract the importance of different bands automatically. **Figure 4** shows the accumulated importance of each band to the output, which is computed by Eq.2. r is the importance vector and it has k elements. Each element r_k represents the importance of the k-th band, w represents the input unit weights extracted from each hidden layer.

$$r = \frac{\sum |w^1||w^2|\cdots|w^M|}{\sum\sum |w^1||w^2|\cdots|w^M|} \quad (2)$$

The importance scores of band 1-7 are shown in Figure 4. We can see that bands 1-6 contribute most to the final output with importance scores larger than 10%. Band 2 contributes the most and band 7 contributes the least. Our feature interpretation result is consistent with band selection in the spectral unmixing algorithm[15] as bands 1-3 show the highest importance scores among the 7 bands. However, our result indicates that besides bands 1-3, bands 4-6 can also provide additional information for melt ponds, ice and open water separation, together covering around 40% of the total contribution to the final output.

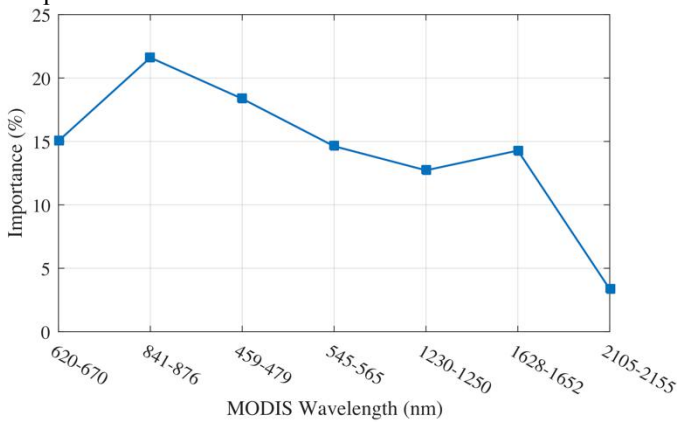

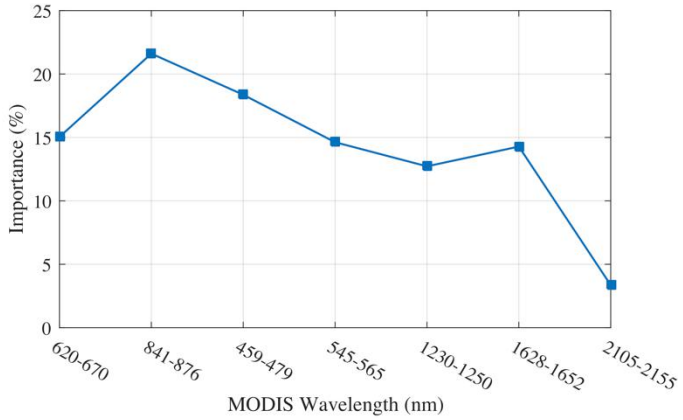

Figure 4. Importance (%) score of each band in differentiating melt ponds from ice and open water.

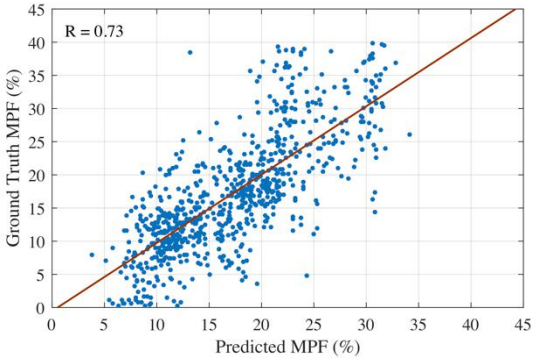

dataset.

Figure 5. Scatter plot showing the MPF retrieved by our MPF-NN model and the ground truth MPF derived from NSIDC

Model Accuracy: A total of 3,925 grids (500 500m) are selected by matching the high-resolution visible images and MODIS data. 70% of them are used for training the model, 10% are used as validation and 20% are used as the test dataset. A 5-fold cross-validation is performed by randomly swapping grids from the test dataset into the training and validation datasets. The model's training process converges in 10,000 epochs. **Figure 5** shows the correlation between MPF retrieved from the trained MPF-NN model and ground truth melt pond fraction derived from NSIDC high-resolution imagery. Overall, our MPF-NN model achieves a RMSE of 3.91% and a correlation coefficient of 0.73.

3.2 Melt pond fraction evolution

Our model is applied to retrieve the MPF at different sites (Beaufort Sea, Canadian Arctic, Fram Strait) and for the whole Arctic. The evolution analysis can illustrate the temporal and spatial variation of melt ponds.

Four Sites: For each site, we select a 10km^2 square area surrounding it to calculate its MPF. Table 1 shows several key statistics such as first peak, second peak and mean MPF. The mean MPF is calculated by averaging the MPF from May to the first week of September except for Beaufort Sea site, where the time period spans from May to the end of July. As it shows, Beaufort Sea has the highest mean MPF (18.22%), while East Siberian has the second highest mean MPF (13.04%), which is slightly higher than the mean MPF in Canadian Arctic and Fram Strait. This result is highly related to the geographical latitudes where those sites are located, as Beaufort Sea has lower latitude than the other three sites.

For occurrence of peaks, we find that the two peaks for Canadian Arctic, East Siberian, and Fram Strait derived from MPF-NN model share similar characteristics with each other. For instance, as shown in Table 1, these three sites have the first peak in early July and the second peak in late July. For Beaufort sea, it reaches the first peak earlier than the other three sites. We also compare our peak result with the Arctic MPF peaks produced by the CICE hindcasts model[8], which has the first peak at July 10th and the second peak at July 16th. Our peak results agree with Arctic overall peaks.

Our MPF-NN model utilizes melt ponds information from multiple sites and multiple time periods. Therefore, the MPF-AN model has the capability to retrieve MPF at each individual site and effectively shows the spatial-temporal

variability of MPF trend.

Arctic: We further evaluate the robustness of the MPF-NN model by retrieving MPF in a different year when the ground truth data for model training is not available. Because of cloud coverage, we select MODIS 500m 8-day surface reflectance products (MOD09A1) instead of daily products to produce the Arctic MPF map during the summer of 2008. The date showing on the figure is the start date of this 8-day period. All cloud pixels are removed. As shown in **Figure 6**, during summer, the general MPF evolution characteristics retrieved by our model is consistent with other models[15,18], which strongly increases in June and July, reaching a value of 20-30%. The minimum MPF appears in May and the end of August which are less than 10%. Also, we notice that melt ponds start later at higher latitude, which agrees with the finding of Zege, E *et al*.[18].

4. Conclusions

In this work, we developed MPF-NN, a novel multi-layer neural network based approach to retrieve MPF from satel-lite data. MPF-NN utilizes multi-site and multi-period high-resolution visible imagery as prior knowledge and hence has a better capability to capture the spatial-temporal variability of melt ponds than single field observation. An automated method was designed to interpret the contribution of different spectral bands by using the weights from hidden layers of MPF-NN. MPF derived from MODIS data using MPF-NN model has a RMSE of 3.91% and a correlation coefficient of 0.73 when compared with validation data, which outperforms the previous spectral unmixing algorithm[15]. It also demonstrates the ability of modeling the melt pond evolution at different sites as well as the Arctic. Finally, though we illustrated the capability of MPF-NN model working with MODIS data, the model can be generalized using various multi-spectral satellite datasets for different parameter retrieval.

Model			**MPF-NN**	
Statistics	Beaufort	Canadian	East Siberian	Fram Strait
Date (1st Peak)	06-27	07-03	07-06	07-12
Data (2nd Peak)	07-23	07-23	07-24	07-23
Mean MPF (%)	18.22	11.24	13.04	11.56

Table 1. Sites MPF statistics

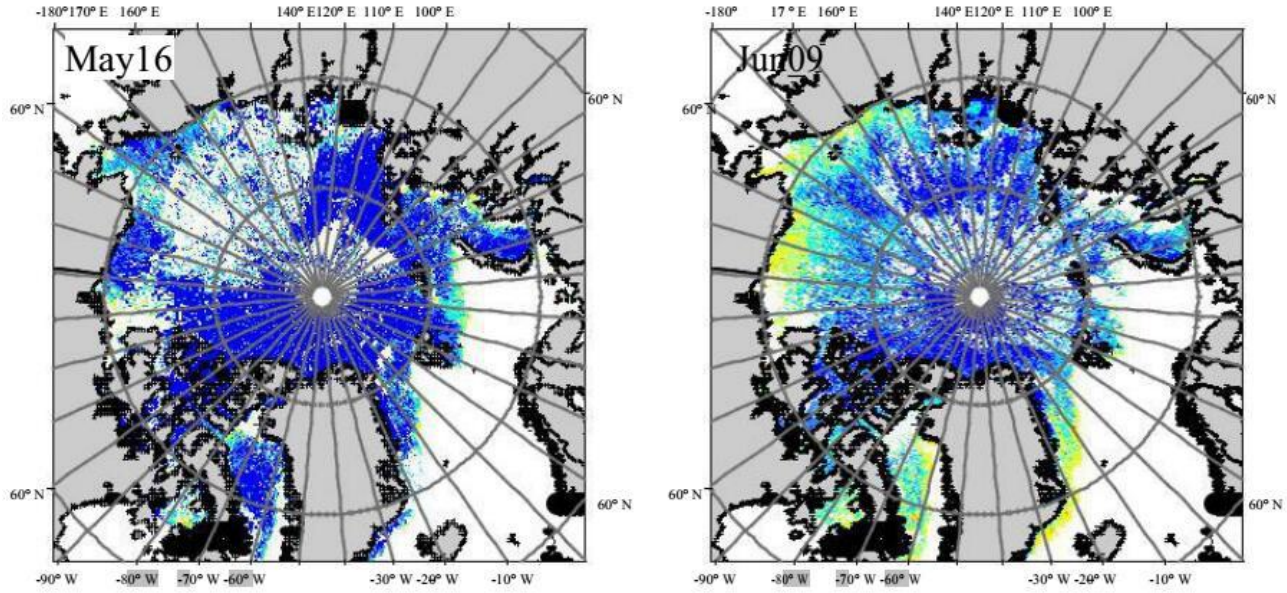

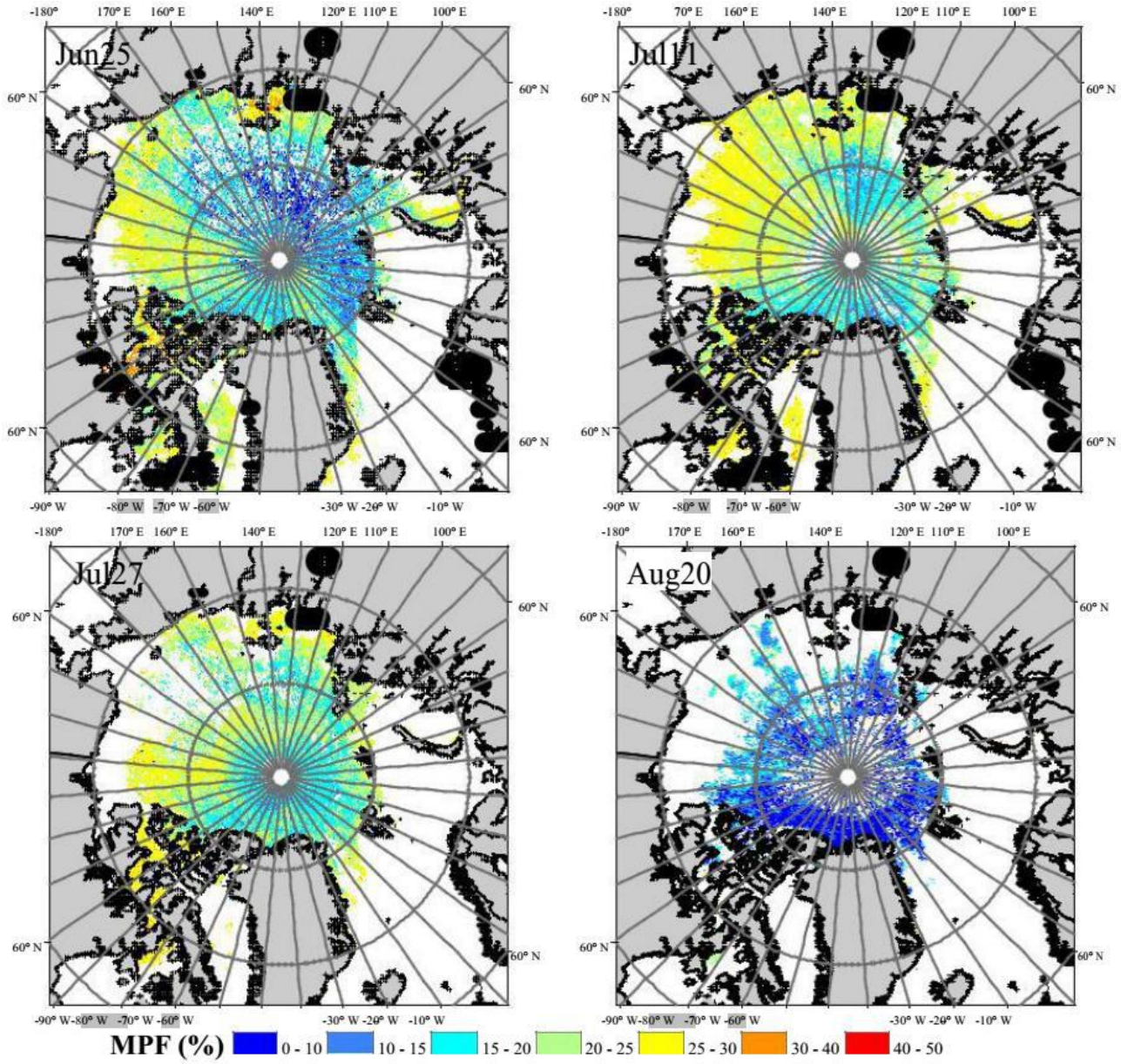

Figure 6. Arctic MPF map in the summer of 2008.

References

1. F Fetterer, N Untersteiner. Observations of melt ponds on arctic sea ice. Journal of Geophysical Research1998; 103(24): 821–24.
2. D Perovich, T Grenfell, B Light, *et al*. Seasonal evolution of the albedo of multiyear arctic sea ice. Journal of Geophysical Research: Oceans 2002; 107(C10).
3. C Polashenski, D Perovich, Z Courville. The mechanisms of sea ice melt pond formation and evolution. Journal of Geophysical Research: Oceans 2012; 117(C1).
4. D Perovich, W Tucker, K Ligett. Aerial observations of the evo-lution of ice surface conditions during summer. Journal of Geophysical Research: Oceans 2002; 107(C10).
5. D Flocco, DL Feltham, AK Turner. Incorporation of a physically based melt pond scheme into the sea ice component of a climate model. Journal of Geophysical Research: Oceans 2010; 115(C8).
6. D Flocco, D Schroeder, DL Feltham, *et al*. Impact of melt ponds on arctic sea ice simulations from 1990 to 2007. Journal of Geophysical Research: Oceans2012; 117(C9).
7. D Schroder, DL Feltham, D Flocco, *et al*. September arctic sea-ice minimum predicted by spring melt-pond fraction. Nature Climate Change 2014; 4(5): 353–357.
8. Y Tanaka, K Tateyama, T Kameda, *et al*. Estimation of melt pond fraction over high-concentration arctic sea ice using amsr e passive microwave data. Journal of Geophysical Research: Oceans 2016; 121(9): 7056–7072.
9. MA Tschudi, JA Maslanik, DK Perovich. Derivation of melt pond coverage on arctic sea ice using modis observations. Remote Sensing of Environment 2008; 112(5): 2605–2614.

10. A Rosel, L Kaleschke. Comparison of different retrieval techniques for melt ponds on arctic sea ice from landsat and modis satellite data. Annals of Glaciology 2011; 52(57): 185–191.
11. DJ Kim, B Hwang, KH Chung, *et al*. Melt pond mapping with high-resolution sar: The first view. Proceedings of the IEEE 2013; 101(3): 748–758.
12. M Makynen, S Kern, A Rosel, *et al*. On the estimation of melt pond fraction on the arctic sea ice with envisat wsm images. IEEE Transactions on Geoscience and Remote Sensing 2014; 52(11): 7366–7379.
13. H Han, J Im, M Kim, *et al*. Retrieval of melt ponds on arctic multiyear sea ice in summer from terrasar-x dual-polarization data using machine learning approaches: A case study in the chukchi sea with mid-incidence angle data. Remote Sensing 2016; 8(1):57.
14. A Rosel, L Kaleschke, G. Birnbaum. Melt ponds on arctic sea ice determined from modis satellite data using an artificial neural network. The Cryosphere 2012; 6(2): 431–446.
15. F Fetterer, S Wilds, J Sloan. Arctic sea ice melt pond statistics and maps, 1999-2001, version 1. [2000 to 2001]. Boulder, Colorado USA: National Snow and Ice Data Center Distributed Active Archive Center, 2008.
16. MA Webster, IG Rigor, DK Perovich, *et al*. Seasonal evolution of melt ponds on arctic sea ice. Journal of Geophysical Research: Oceans 2015; 120(9): 5968–5982.
17. E Zege, A Malinka, I Katsev, *et al*. Algorithm to retrieve the melt pond fraction and the spectral albedo of arctic summer ice from satellite optical data. Remote Sensing of Environment 2015; 163: 153–164.
18. L Istomina, G Heygster, M Huntemann, *et al*. Melt pond fraction and spectral sea ice albedo retrieval from meris data-part 1: Validation against in situ, aerial, and ship cruise data. The Cryosphere 2015; 9: 1551–1566.
19. Y LeCun, Y Bengio, G Hinton. Deep learning. Nature 2015; 521(7553): 436–444.
20. K Hornik. Approximation capabilities of multilayer feedforward net-works. Neural networks 1991; 4(2): 251–257, 1991.
21. J Li, X Li, B Huang, *et al*. Hopfield neural network approach for supervised nonlinear spectral unmixing. IEEE Geoscience and Remote Sensing Letters 2016 July; 13(7): 1002–1006.
22. D Kingma, J Ba. Adam: A method for stochastic optimization. arXiv preprint arXiv:1412.6980, 2014.
23. N Srivastava, GE Hinton, A Krizhevsky, *et al*. Dropout: a simple way to prevent neural networks from overfitting. Journal of Machine Learning Research 2014; 15(1): 1929–1958.
24. DK Perovich, C Polashenski. Albedo evolution of seasonal arctic sea ice. Geophysical Research Letters2012; 39(8).